

Article

Synthesis of Monoclinic Vanadium Dioxide via One-Pot Hydrothermal Route

Guowei Liu ^{1,2,†}, Zengyan Du ^{3,4,†}, Ming Li ^{3,*} and Yi Long ^{1,2,5,*}

¹ School of Materials Science and Engineering, Nanyang Technological University, 50 Nanyang Avenue, Singapore 639798, Singapore; gliu003@e.ntu.edu.sg

² Singapore-HUJ Alliance for Research and Enterprise (SHARE), Campus for Research Excellence and Technological Enterprise (CREATE), Singapore 138602, Singapore

³ Key Laboratory of Materials Physics, Anhui Key Laboratory of Nanomaterials and Nanotechnology, Institute of Solid State Physics, Chinese Academy of Sciences, Hefei 230031, China; zydu@mail.ustc.edu.cn

⁴ School of Chemistry and Materials Science, University of Science and Technology of China, Hefei 230026, China

⁵ Sino-Singapore International Joint Research Institute (SSIJRI), Guangzhou 510000, China

* Correspondence: liming@issp.ac.cn (M.L.); longyi@ntu.edu.sg (Y.L.)

† These authors contributed equally to this work.

Abstract: Pure monoclinic vanadium dioxide nanoparticles (VO₂ NPs) with a controlled uniform size are considered essential for the preparation of thermochromic smart window coatings on desired substrates. Herein, we report a facile one-step hydrothermal synthesis of VO₂(M) NPs without post-treatment of annealing, which may induce unwanted aggregation of NPs. In contrast with the annealed sample, the one-step processed VO₂(M) NPs exhibit superior thermochromic performance with the solar modulation efficiency of 11.8% and luminous transmittance of 37.3%.

Keywords: hydrothermal; one-step; single-phase; thermochromic



Citation: Liu, G.; Du, Z.; Li, M.; Long, Y. Synthesis of Monoclinic Vanadium Dioxide via One-Pot Hydrothermal Route. *Colloids Interfaces* **2021**, *5*, 13. <https://doi.org/10.3390/colloids5010013>

Academic Editors:
Alexander Kamyshny and
Victor Starov

Received: 15 January 2021
Accepted: 10 February 2021
Published: 16 February 2021

Publisher's Note: MDPI stays neutral with regard to jurisdictional claims in published maps and institutional affiliations.



Copyright: © 2021 by the authors. Licensee MDPI, Basel, Switzerland. This article is an open access article distributed under the terms and conditions of the Creative Commons Attribution (CC BY) license (<https://creativecommons.org/licenses/by/4.0/>).

1. Introduction

Vanadium dioxide (VO₂), as a typical strongly electron-correlated transition metal oxide, has a first-order and reversible metal–insulator transition (MIT) at phase transition temperature (τ_c) ~340 K. The MIT was first discovered by Morin et al. in 1959 [1]. Since then, it has drawn extensive research [2]. At room temperature and unstrained, the crystal structure of VO₂ is monoclinic (M, P2₁/c, a = 5.75 b = 4.54 c = 5.38, β = 122.64°) with zig-zag dimerized V–V pairs along c axis, while above the τ_c , a tetragonal structure (7 P4₂/mnm a = b = 4.55 c = 2.86, β = 90°) is favored. The MIT happens within 1 ps [3], accompanied by an abrupt electrical resistance change of approximately five orders of magnitude [4]. As well as changes of structure and electrical properties, the abrupt optical modulation in the wavelength of infrared [5], terahertz [6], and microwave [7] during MIT gives VO₂ great potential for applications such as thermochromic smart windows [8], 3D-printed smart window [9], optical switching devices [10], light modulator [11], and infrared stealth [12].

The key to realizing these intensive applications depends on the controlled preparation of high-quality VO₂ single/polycrystals powders or thin-film due to the multivalent nature of vanadium element, making it tough work to synthesize high purity VO₂. Compared with some high-cost or complex methods, such as electrodeposition [13], sputtering [14], pulse laser [15], and sol-gel [16], hydrothermal synthesis is probably the most effective method to control the morphology, size, and phase structures of VO₂. Recently, Li et al. summarized a detailed review on the hydrothermal synthesis of the VO₂ phase and its application in thermochromic smart windows [17], from which we know that most of the reported one-step hydrothermal syntheses require a high temperature and long reaction time. Meanwhile, in most cases, certain metal doping, such as tungsten [18,19], is necessary to obtain VO₂(M) nanoparticles (NPs). However, the doping elements that substitute

vanadium elements normally deteriorate the crystallinity and hinder the thermochromic performance of VO₂. Son et al. prepared the VO₂(M) phase with different morphologies by changing hydrothermal temperatures, pH value, and duration [20]. However, the product was generally a mixture of the two phases, which is not suitable for the actual applications. Chen et al. synthesized the fine crystalline VO₂(M) NPs via one-step hydrothermal, and they found both a high latent heat of 43 J/g and good thermochromic property of the VO₂ in comparison to the bulk one [21]. However, the used high hydrothermal temperature, up to around 400 °C, leads to a high cost and uneven size distribution of VO₂ NPs. Alie et al. also reported the direct hydrothermal synthesis of VO₂ without doping via modifying the molar ratio of oxalic acid and V₂O₅ [22]. The obtained VO₂ microcrystals showed a mixture of star shape and hollow sphere shape. The use of seed-assisted one-step hydrothermal to form VO₂ composite has also been recently reported by Jin et al. They reported a novel VO₂-ZnO dandelion structure with the help of the TiO₂ seeds [23]. Li et al. synthesized TiO₂ seeds assisted Mo-doped VO₂ zero-dimensional NPs due to the low nucleation energy [24]. A novel one-step hydrothermal was invented by Guo et al., in which they separated the hydrogen peroxide from the precursor solution, providing a rational oxidizing hydrothermal system [25]. However, the duration of hydrothermal synthesis has been doubled at the same time. Powell et al. and Malarde et al. introduced a continuous hydrothermal flow synthesis method for the direct preparation of a large amount VO₂(M) without a post-annealing process, while the mixing temperature synthesis was more than 400 °C [26,27]. Although the continuous hydrothermal synthesis showed a great value towards the industrial procedure, the as-prepared VO₂ NPs exhibited inferior thermochromic performance, proving the poor crystallinity and quality of the product in general.

In this paper, we successfully synthesize non-doping VO₂(M) NPs via one-step hydrothermal at a relatively low temperature within a short time by adjusting hydrothermal parameters, including the amount of the reduction, reaction time, and precursor concentration. The obtained VO₂(M) has evenly distributed uniform size and morphology without further annealing treatment, which displays high crystallinity and good thermochromic performance.

2. Materials and Methods

2.1. Materials and Synthesis

In the experiments, all chemicals of V₂O₅ (Alfa Aesar, Ward Hill, MA, USA, 99.6%), N₂H₄·H₂O (Alfa Aesar, Ward Hill, MA, USA, 99.9%), and H₂O₂ (30 wt%, Sigma-Aldrich, St. Louis, MI, USA) were used as received without any further purification. In a typical hydrothermal process, 1 mmol commercial V₂O₅ powders were added into 5 mL preheated H₂O₂ (30 wt%) at 90 °C with 200 rpm stirring. After a vigorous reaction, a brownish V₂O₅-H₂O₂ precursor was obtained. A certain amount of deionized (DI) water was added subsequently. Afterward, the brownish precursor was chemically reduced by adding N₂H₄·H₂O solution dropwise with stirring for 10 min. After the precursor turned blue-black, it was transferred into a 50 mL PTFE liner and sealed in a stainless steel autoclave. The hydrothermal temperature was set at 260 °C for a certain period (12–168 h), and then the samples were cooled to room temperature in the air. The black precipitate was collected by centrifugation and washed several times in turn with DI water, acetone, and ethanol. After being dried at 50 °C in a vacuum oven, the final black powders were obtained. No further annealing process was performed on any of the products.

2.2. Preparation of VO₂-Based Thermochromic Film

The 50 mg of as-prepared VO₂ NPs were evenly dispersed into 5 mL ethanol and 5 mL concentrated Si-Al solution by one-hour ultrasonication bath. The synthesis of the Si-Al solution has been reported in our previous work [8]. The VO₂ films were further prepared by spin coating on the soda-lime glass substrate with the same speed and coating times.

The coated substrate was dried in the vacuum oven for one hour at 90 °C, then another one hour at 150 °C to remove the solvent and form the uniform coatings.

2.3. Characterization

The X-ray diffraction (XRD) patterns of the obtained powders were collected from a Shimadzu Powder XRD-6000 X-ray diffractometer with Cu K α radiation ($\lambda = 0.15406$ nm) under 40 KV voltage and 30 mA current. The surface morphology of the samples was characterized by field emission scanning electron microscope (FESEM, JSM-7600F, JEOL, Akishima, Tokyo, Japan). Differential Scanning Calorimeter (DSC Q10, TA instrument, New Castle, DE, USA) was used to characterize the phase transition behavior of the samples upon the heating and cooling rate of 10 °C/min under N₂ atmosphere. Variable temperature optical transmission spectra of the prepared VO₂ films were measured on a UV-Vis-NIR spectrophotometer (Cary 5000, Agilent Ltd., Santa Clara, CA, USA) in the wavelength of 250–2500 nm at 20 and 90 °C, respectively. A Linkam PE120 system Peltier heating and the cooling stage was attached to regulate the temperature of the substrates. The integrated luminance transmittance and solar transmittance were calculated using the below expression based on the transmittance data:

$$T_{\text{lum/sol}} = \frac{\int \phi_{\text{lum/sol}}(\lambda)T(\lambda)d\lambda}{\int \phi_{\text{lum/sol}}(\lambda)d\lambda}$$

$$\Delta T_{\text{sol}} = \frac{\int \phi_{\text{lum/sol}}(\lambda)T(\lambda)d\lambda}{\int \phi_{\text{lum/sol}}(\lambda)d\lambda}$$

where $T(\lambda)$ denotes the film transmittance data at wavelength λ , ϕ is the solar irradiance spectrum for air mass 1.5 (corresponding to the sun standing 37° above the horizon). A more detailed discussion on the evaluation method was reported in [28].

3. Results and Discussion

3.1. Effect of the Amount of the Reduction

As discussed in our previous paper [29], the amount of reduction is the crucial factor for the synthesis of VO₂ phase. Thus, in a series of hydrothermal experiments, the amount of N₂H₄·H₂O solution was optimized first.

The XRD patterns of the hydrothermal samples under the same condition, but with different amounts of the reduction, are shown in Figure 1. The crystallography data are listed in Table 1. The phase evolution of the obtained vanadium oxide could be observed from the increment of the reduction. When the initial amount of N₂H₄·H₂O was 30 μ L, the hydrothermal product was still V₂O₅, which is the same phase as the raw material. This is due to the fact that the reduction was mainly consumed by the residual H₂O₂ in the precursor. After the amount of N₂H₄·H₂O increased to 50 μ L, the V₂O₅ was reduced to pure V₆O₁₃. When 60 μ L of N₂H₄·H₂O was selected, a high crystalline pure phase of VO₂(M) (JCPDS #43-1051) was synthesized. The pure VO₂(M) was still retained when the amount of reduction increased to 70 μ L, but from the XRD pattern, the crystallinity of the product became much lower. As shown in Figure 1e,f, the powders were reduced to V₆O₁₁ and V₃O₅, upon which the amount of reduction was further raised to 80 and 90 μ L. Additionally, the crystallinity of the powders gradually decreased with increment of N₂H₄·H₂O no matter what kind of vanadium oxide phase it was. Therefore, to synthesize the VO₂ NPs with high crystallinity, 60 μ L reduction was chosen as the standard amount for the consequent hydrothermal synthesis.

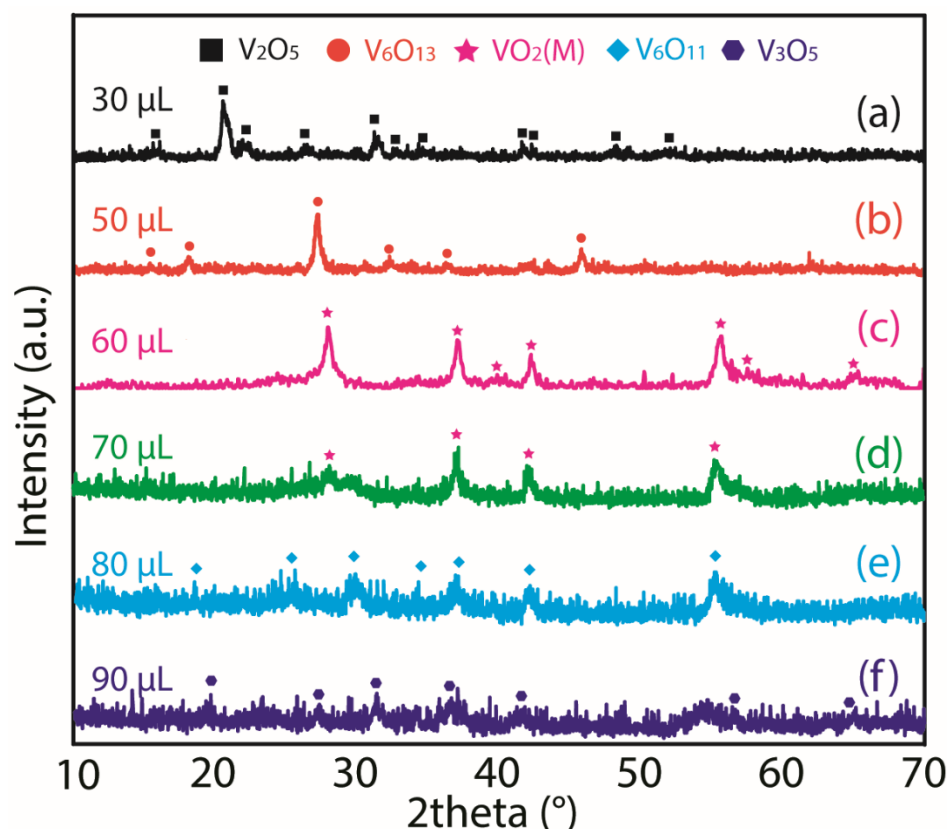


Figure 1. (a–f) XRD patterns of hydrothermal samples with different amounts of the reductive reagent $\text{N}_2\text{H}_4 \cdot \text{H}_2\text{O}$ at 260°C and 24 h duration.

Table 1. The crystallography data of the obtained phases with different amounts of the reductive reagent.

Obtained Sample	Space Group	Cell Parameters a, b, c (Å)	β (°)
V_2O_5 (30 μL)	Pmmn	11.516, 3.565, 4.3727	90
V_6O_{13} (50 μL)	C2/m	11.960, 3.713, 10.070	100.9
$\text{VO}_2(\text{M})$ 60 μL , 70 μL	$\text{P}2_1/\text{c}$	5.752, 4.538, 5.383	122.64
V_6O_{11} (80 μL)	P-1	5.440, 6.990, 23.660	120.9
V_3O_5 (90 μL)	$\text{P}2/\text{c}$	9.835, 5.031, 6.9742	109.46

The morphology of the above samples is shown in Figure 2a–e. With the phase evolution of the obtained vanadium oxides, the morphology of these samples changes from nanowires/microwires dramatically into sub-100 nm NPs and further growth into larger particles. In Figure 2a, the length of V_2O_5 nanowires is up to several micrometers, which is different from the sheet structure of $\text{V}_2\text{O}_5\text{-H}_2\text{O}_2$ precursor both in size and shape reported before [30]. Figure 2b shows the microbelt structure of the obtained V_6O_{13} powder, which is caused by the aggregation of the initially formed nanowires under hydrothermal conditions. Simultaneously, small amounts of the NPs could be observed at the edge of the microwire. From Figure 2c, the morphology of the VO_2 product is the uniform NPs with a diameter around 100 nm. No nanowire or micrometer was observed. Upon further adding the reduction, the size of the particles is getting larger and irregular, from NPs to micrometer bulks, as shown in Figure 2d,e. The irregular morphology also causes a decrease in the crystallinity, as discussed in Figure 1 of the XRD results.

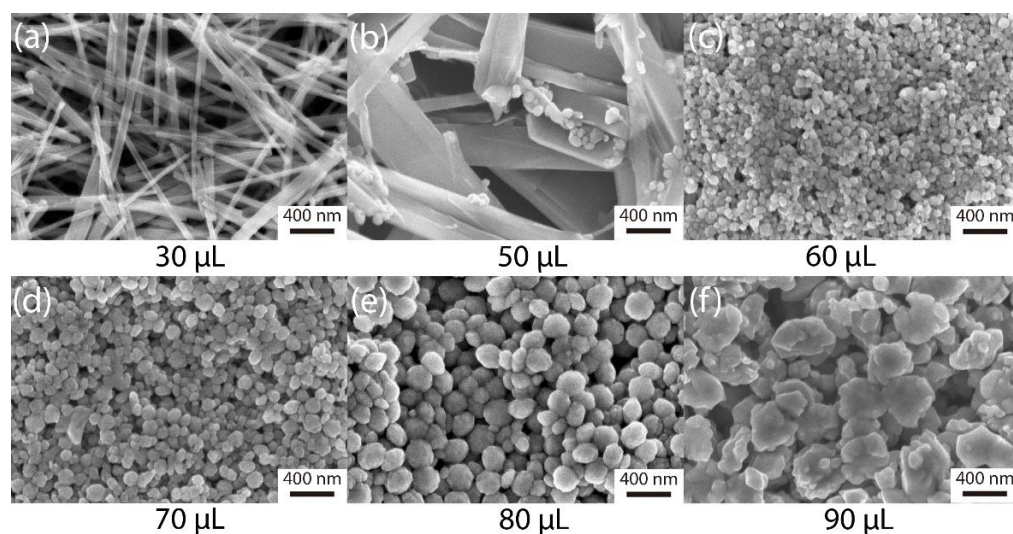


Figure 2. (a–f) SEM images of hydrothermal samples with different amounts of the reduction at 260 °C and 24 h duration.

Based on Figures 1 and 2, a hydrothermal synthesis mechanism could be speculated. With the high temperature and pressure, the sheet structure of the precursor turned into nanowires at the initial stage. The reduction process began with the increased amount of $N_2H_4 \cdot H_2O$. The nanowires grew together into the microwires via an oriented attachment mechanism, and then the NPs gradually appeared at the edge of the microwires. The final morphology using $N_2H_4 \cdot H_2O$ as the reduction of the VO_2 was NPs, which is similar to the previous reports. Herein, $N_2H_4 \cdot H_2O$ plays a crucial role in the hydrothermal process of VO_2 (M), which provides a reducing environment and controls the phase and morphology of the NPs. Gui et al. speculated a molecular coordination mechanism, and the hydrazine and vanadium could be assembled as a building block and promote the growth of the particle-shape VO_2 nanocrystalline [31]. The same group further synthesized nanorod VO_2 (R) via adding hydrazine, and they further postulated that hydrazine could serve as a soft template. Both Santulli et al. and Son et al. found the potential of N_2H_4 as the coordination agent in central vanadium ions into one-dimensional nanorod, nanoneedle morphologies [20]. Additionally, Ji et al. postulated that with the existence of N_2H_4 , the $[V_2O_7]^{4-}$ was the main vanadium complex, while with the presence of $H_2C_2O_4$, the dominant vanadium complex was larger volume $[V_{10}O_{28}]^{6-}$, in which micro-size particles were favorably produced [32].

3.2. Effect of the Hydrothermal Duration

The second parameter discussed in the series of the hydrothermal preparation was the hydrothermal duration while keeping $N_2H_4 \cdot H_2O$ at 60 μ L. The XRD results in Figure 3 show that the hydrothermal samples with different duration increased from 12 h to 168 h. It can be found that all samples are single-phase VO_2 (M) when the reduction amount was kept constant. The XRD peaks of the VO_2 (M) gradually intensified with the increase of the hydrothermal duration.

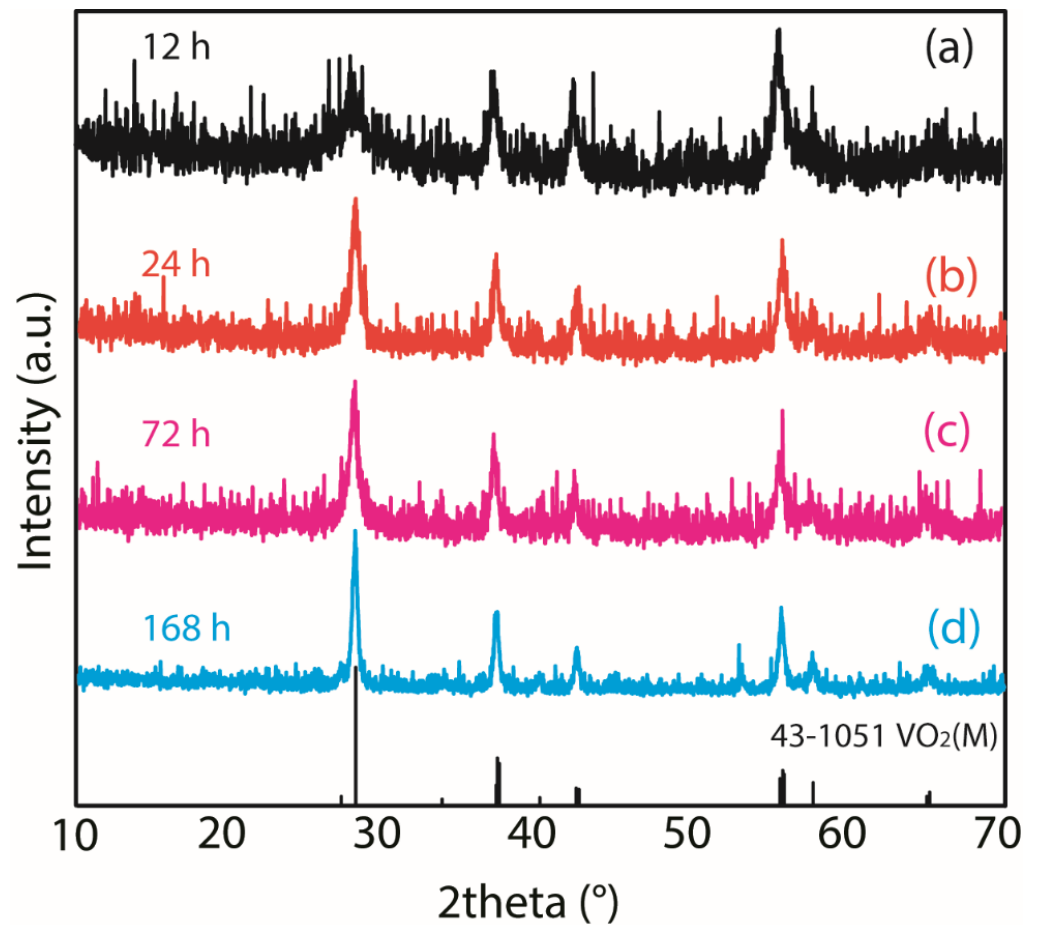


Figure 3. (a–d) XRD patterns of hydrothermal samples with different duration at 260 °C with 60 μ L $N_2H_4 \cdot H_2O$.

Figure 4a shows a large amount of the hollow half-sphere shape within 12 h hydrothermal synthesis, which indicates that a short time less than 12 h was far from enough for the growth of uniform NPs, and the size of the particles were rather uneven, ranging from 20 nm to 130 nm. With the increase in hydrothermal duration to 24 h, the uniform NPs morphology is shown in Figure 4b, with an average size of 60.2 nm. As shown in Figure 4c,d, the hydrothermal duration continued to be extended, the shape of the NPs remained the same, and the size grew larger. The average size was 75.9 nm for the 72 h sample, while the size of NPs grew to nearly 90 nm at an even longer duration at 168 h.

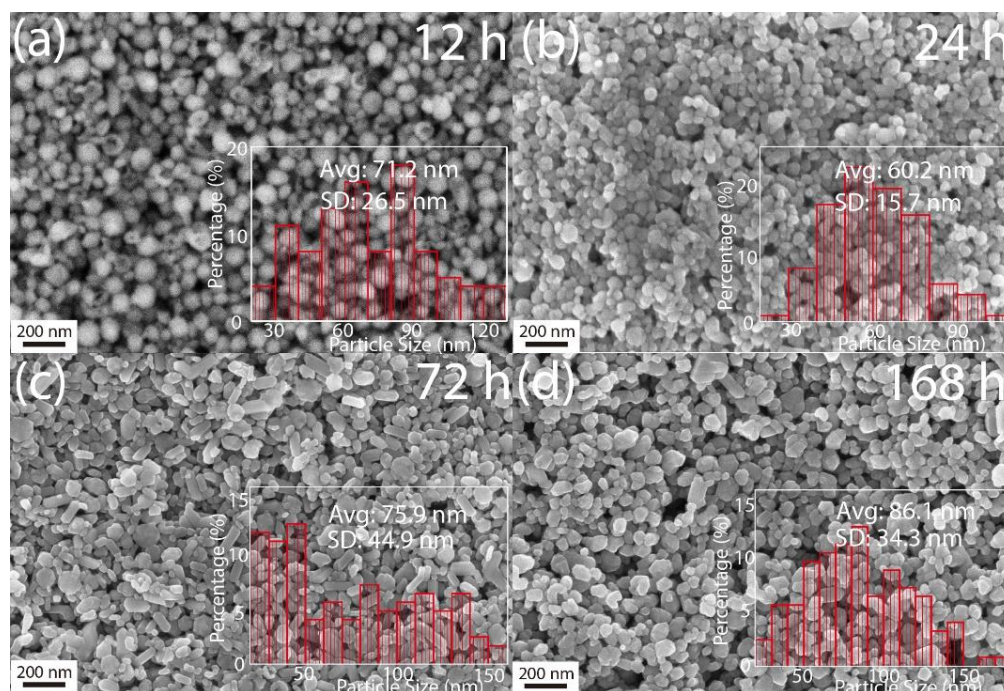


Figure 4. (a–d) SEM images of hydrothermal samples with different duration at 260 °C with 60 μL $\text{N}_2\text{H}_4 \cdot \text{H}_2\text{O}$, inset with the size distribution analysis.

3.3. Effect of the Precursor Concentration

Besides the reduction amount and hydrothermal duration, the precursor concentration is the last hydrothermal parameter we were concerned with in our experiment. The preparation of the precursor was introduced in the experimental section. To adjust the precursor concentration, the volume of the solvent, including H_2O_2 and DI water, was kept unchanged, while the amount of the raw material of V_2O_5 powder was tuned from 1 mmol up to 2 mmol accordingly.

Figure 5 shows the XRD patterns of the hydrothermal samples with different precursor concentrations. The crystallography data are listed in Table 2. Note that the concentration of V_2O_5 powder was kept at 1 mmol in our experiment as mentioned above. As shown in Figure 5b, all of the XRD peaks are attributed to the standard $\text{VO}_2(\text{M})$ peaks. Two uncertain peaks marked with the star, around 18.7° and 37.8° , turned up as we increased the concentration of V_2O_5 up to 1.25 mmol (Figure 5b). Upon further increasing the V_2O_5 concentration to 1.5 mmol, Figure 5c exhibits that most of the peaks are assigned to $\text{VO}_2(\text{B})$, although a small number of peaks attributed to $\text{VO}_2(\text{M})$ could still be observed. When the concentration of V_2O_5 powder was increased to 2 mmol, V_6O_{13} was synthesized, as shown in Figure 5d. However, there were still $\text{VO}_2(\text{M})$ peaks. This suggests that the reduction amount is significant to synthesize the $\text{VO}_2(\text{M})$, while the precursor concentration must be controlled within the corresponding range.

Table 2. The crystallography data of the obtained phases with different precursor concentrations.

Obtained Sample	Space Group	Cell Parameters a, b, c (Å)	β (°)
$\text{VO}_2(\text{M})$	$\text{P}2_1/\text{c}$	5.752, 4.538, 5.383	122.64
$\text{VO}_2(\text{B})$	$\text{C}2/\text{m}$	12.152, 3.719, 6.347	107.58
V_6O_{13}	$\text{C}2/\text{m}$	11.960, 3.713, 10.070	100.9

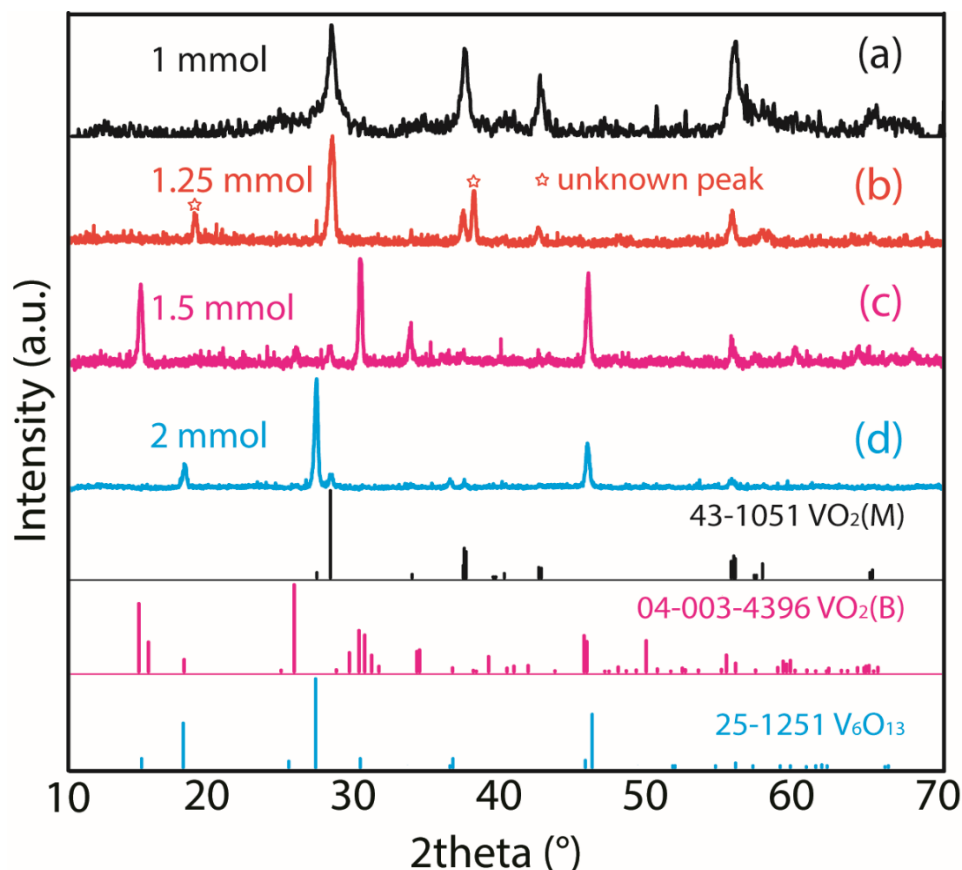


Figure 5. (a–d) XRD patterns of hydrothermal samples with different precursor concentrations at 260 °C with 60 μL $\text{N}_2\text{H}_4 \cdot \text{H}_2\text{O}$ and 24 h duration. Stars in Figure 5b indicate the unknown peaks.

The SEM images in Figure 6 shows morphologies of the above samples, which highly coincided with the XRD results. Figure 6a shows the highly uniform NPs, which is the pure $\text{VO}_2(\text{M})$ phase. In Figure 6b, two shapes of the particles are clearly shown. The NPs are $\text{VO}_2(\text{M})$, while the thicker nanobeams mostly belong to the unknown phase indicated in the XRD pattern (Figure 5b). Two different kinds of morphology in NPs and ultralong nanowires are shown in Figure 6c. According to the XRD results, the nanowires with lengths up to several micrometers belong to $\text{VO}_2(\text{B})$, while the NPs are $\text{VO}_2(\text{M})$. In Figure 6d, it is found that besides the $\text{VO}_2(\text{M})$ NPs, microbelts are observed. The microbelts comprise V_6O_{13} , based on the XRD result, which is completely identified as the V_6O_{13} in Figure 2b.

3.4. Thermochromic Performance of $\text{VO}_2(\text{M})$ NPs

Figure 7 shows the DSC of the synthesized VO_2 NPs from different hydrothermal durations in the hydrothermal process. In general, endothermic peaks are observed in the heating segment, while exothermal peaks are found during the cooling process, and the thermal hysteresis indicates that the VO_2 possesses first-order and fully reversible phase transition. The transition temperature and enthalpy of the samples were integrated by the collected data and determined by the TA analysis software.

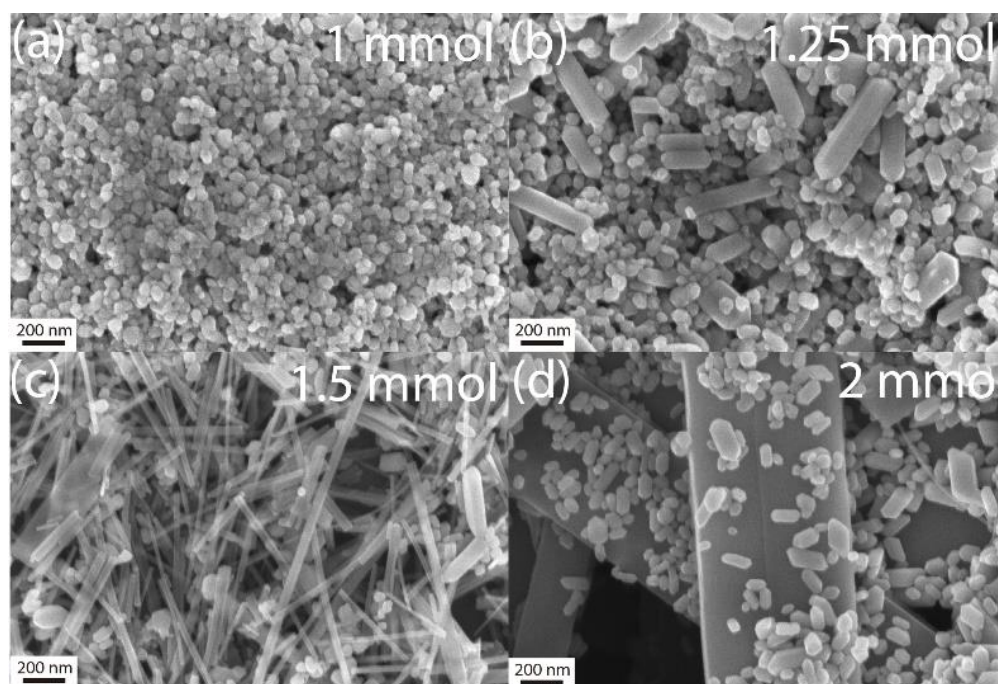


Figure 6. (a–d) SEM images of hydrothermal samples with different precursor concentrations at 260 °C with 60 μL $\text{N}_2\text{H}_4 \cdot \text{H}_2\text{O}$ and 24 h duration.

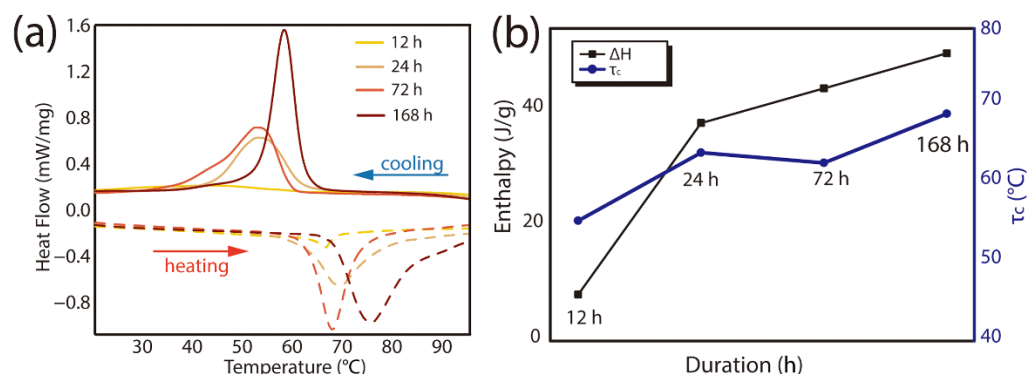


Figure 7. (a) Differential Scanning Calorimeter (DSC) curves of the hydrothermal VO_2 powders at different hydrothermal duration at 260 °C with 60 μL $\text{N}_2\text{H}_4 \cdot \text{H}_2\text{O}$; (b) phase change enthalpy (ΔH) and transition temperature (τ_c) versus hydrothermal duration.

In Figure 7a, the 12 h hydrothermal sample barely exhibits any peaks. The bump appears at 66.2 °C during the heating ramp and at 43.4 °C during the cooling ramp. The transition temperature was 54.8 °C, and the latent heat is 7.6 J/g, much lower than the reported data [17]. This suggests a large number of defects in the samples, and it further proves that the insufficient hydrothermal time for the VO_2 synthesis, as discussed in Figure 4a. As the duration increased to 24 h, the endothermic and exothermic peaks were both shifted towards the higher temperature, that is, 70.2 °C and 56.5 °C, which brought the τ_c to 63.4 °C, and the enthalpy increased to 37.3 J/g. As for the 72 h hydrothermal sample, the position of the peaks barely shifted, while the enthalpy further increased to 43.3 J/g. A more significant change for DSC peaks could be observed for the 168 h duration sample. The endothermic peak appeared at 77.4 °C and the exothermic bump at 59.2 °C, which puts the τ_c at 68.3 °C. The obtained enthalpy value was 49.4 J/g. In contrast, the endothermic or exothermic peaks for 72 h and 168 h are sharper, indicating the larger particle size for these samples (Figure 4). The trend that ΔH and τ_c both increased with the longer hydrothermal duration is further shown in Figure 7b.

The thermochromic property is evaluated through the temperature-dependent UV-Vis-NIR spectra, as shown in Figure 8. The solid and dotted lines demonstrate the high temperature and low-temperature optical transmittance, respectively, of the prepared VO₂ films. Figure 8a shows all three samples with different concentrations of VO₂ dispersion prepared from the non-doped single-phase VO₂ NPs. The concentration of the prepared VO₂ dispersion was adjusted by the added amount of the VO₂ powders, and the volume of the solvent, including alcohol and Si-Al gel, was kept the same. The thickness of the three samples was also kept the same by controlling the same speed and time of the spin-coating process. For the 1% film, the integrated luminous transmittance (T_{lum}) was calculated to be 44.4%, and the solar modulation (ΔT_{sol}) was 10.4%. With the higher concentration of the dispersion, the solar modulating ability was improved alongside the degradation of the T_{lum} (2% sample, $T_{lum} \sim 37.3\%$, $\Delta T_{sol} \sim 11.8\%$, and 3% sample, $T_{lum} \sim 13.8\%$, $\Delta T_{sol} \sim 13.6\%$). The thermochromic performances of the hydrothermal samples of different durations are exhibited in Figure 8b. All samples were made with the same concentration of VO₂ dispersion, as well as the same film thickness. With the duration increased to 72 h and 168 h, the blueshift of the crosspoint between the low and high temperature can be observed in the transmittance spectra, as shown in the circles of Figure 8b. This is caused by the different optical scattering properties between the room temperature VO₂(M) and high-temperature phase VO₂(R). The higher transmittance in the visible wavelength range is due to the less light scattered in the high-temperature VO₂(R). With the longer hydrothermal duration, crosspoints appear for the 72 h sample with particle size at 75.9 nm and the 168 h sample with 86.1 nm. This phenomenon deteriorates the thermochromic performance of the longer duration sample (72 h sample, $T_{lum} \sim 31.7\%$, $\Delta T_{sol} \sim 11.0\%$, and 168 h sample, $T_{lum} \sim 35.7\%$, $\Delta T_{sol} \sim 5.7\%$) compared with the 24 h sample at the same thickness and dispersion concentration ($T_{lum} \sim 37.3\%$, $\Delta T_{sol} \sim 11.8\%$).

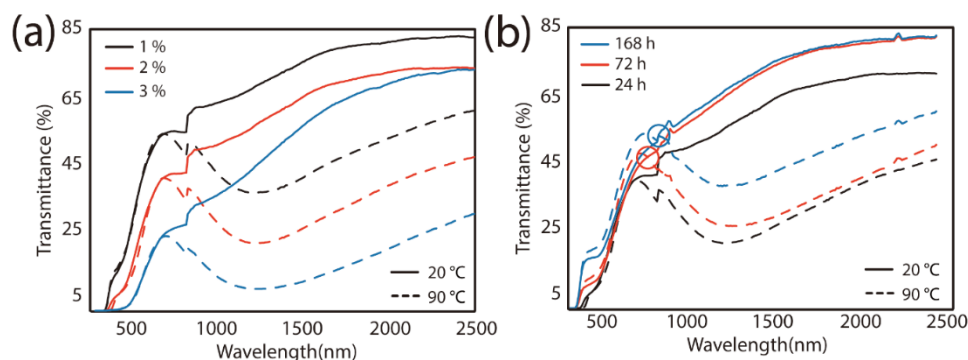


Figure 8. Transmittance spectra of fabricated VO₂ films with VO₂ nanoparticles (NPs) synthesized: (a) different concentrations of prepared VO₂ dispersion; (b) different duration of the hydrothermal samples. The circles in the figure indicate the appearance of the crosspoints.

4. Conclusions

In this paper, pure VO₂(M) NPs with uniform morphology were prepared via one-step hydrothermal synthesis without doping or annealing treatment. The raw material of V₂O₅ was gradually reduced to microbelt V₆O₁₃ and then to desired VO₂ NPs, and eventually to larger and irregular morphology V₆O₁₁ and V₃O₅ with the increment of the N₂H₄·H₂O addition. Furthermore, hydrothermal duration and precursor concentration have been studied carefully to obtain the pure and high crystallinity NPs. The obtained VO₂ powders were dispersed and spin-coated onto glass substrates to prepare VO₂ films, which exhibited comparable thermochromic performance. This provides an alternative way to understand the hydrothermal process mechanism for synthesizing the multi-phase and multi-valence vanadium oxides. The proposed hydrothermal method could be extended for various vanadium oxides synthesis in applications beyond smart window coatings.

Author Contributions: Conceptualization, G.L. and Z.D.; methodology, G.L. and Z.D.; validation, G.L., Z.D., M.L. and Y.L.; investigation, G.L. and Z.D.; data curation, G.L. and Z.D.; writing—original draft preparation, G.L. and Z.D.; writing—review and editing, M.L. and Y.L.; supervision, Y.L. All authors have read and agreed to the published version of the manuscript.

Funding: This research was funded by Singapore Ministry of Education (MOE) Academic Research Fund Tier one RG103/19 and the National Research Foundation, Prime Minister's Office, Singapore under its Campus for Research Excellence and Technological Enterprise (CREATE) program.

Data Availability Statement: All the data has included in the article.

Acknowledgments: The principal investigator of this project (Y.L.) wishes to thank Sino-Singapore International Joint Research Institute for funding support. This research was supported by Singapore Ministry of Education (MOE) Academic Research Fund Tier one RG103/19 and the National Research Foundation, Prime Minister's Office, Singapore under its Campus for Research Excellence and Technological Enterprise (CREATE) program. Y.L. sincerely thanks the generous funding support from Freddy Y.C. Boey.

Conflicts of Interest: The authors declare no conflict of interest.

References

1. Morin, F.J. Oxides Which Show a Metal-to-Insulator Transition at the Neel Temperature. *Phys. Rev. Lett.* **1959**, *3*, 34–36. [[CrossRef](#)]
2. Ke, Y.; Wang, S.; Liu, G.; Li, M.; Hite, T.J.; Long, Y. Vanadium Dioxide: The Multistimuli Responsive Material and Its Applications. *Small* **2018**, *14*, e1802025. [[CrossRef](#)] [[PubMed](#)]
3. Gray, A.X.; Hoffmann, M.C.; Jeong, J.; Aetukuri, N.P.; Zhu, D.; Hwang, H.Y.; Brandt, N.C.; Wen, H.; Sternbach, A.J.; Bonetti, S.; et al. Ultrafast terahertz field control of electronic and structural interactions in vanadium dioxide. *Phys. Rev. B* **2018**, *98*, 045104. [[CrossRef](#)]
4. Berglund, C.N.; Guggenheim, H.J. Electronic Properties of VO₂ near the Semiconductor-Metal Transition. *Phys. Rev.* **1969**, *185*, 1022–1033. [[CrossRef](#)]
5. Ran, K.; Huang, W.; Shi, Q.; Tang, L.; Peng, B.; Liang, S.; Zhu, H.; Mao, Z. Freeze-drying induced nanocrystallization of VO₂ (M) with improved mid-infrared switching properties. *J. Alloy. Compd.* **2017**, *728*, 1076–1082. [[CrossRef](#)]
6. Lourembam, J.; Srivastava, A.; La-O-Vorakiat, C.; Rotella, H.; Venkatesan, T.; Chia, E.E. New insights into the diverse electronic phases of a novel vanadium dioxide polymorph: A terahertz spectroscopy study. *Sci. Rep.* **2015**, *5*, 9182. [[CrossRef](#)] [[PubMed](#)]
7. Lv, W.; Huang, D.; Chen, Y.; Qiu, Q.; Luo, Z. Synthesis and characterization of Mo–W co-doped VO₂(R) nano-powders by the microwave-assisted hydrothermal method. *Ceram. Int.* **2014**, *40*, 12661–12668. [[CrossRef](#)]
8. Ke, Y.; Yin, Y.; Zhang, Q.; Tan, Y.; Hu, P.; Wang, S.; Tang, Y.; Zhou, Y.; Wen, X.; Wu, S.; et al. Adaptive Thermochromic Windows from Active Plasmonic Elastomers. *Joule* **2019**, *3*, 858–871. [[CrossRef](#)]
9. Zhou, C.; Li, D.; Tan, Y.; Ke, Y.; Wang, S.; Zhou, Y.; Liu, G.; Wu, S.; Peng, J.; Li, A.; et al. 3D Printed Smart Windows for Adaptive Solar Modulations. *Adv. Opt. Mater.* **2020**, 2000013. [[CrossRef](#)]
10. Zhou, Y.; Wang, S.; Peng, J.; Tan, Y.; Li, C.; Boey, F.Y.C.; Long, Y. Liquid Thermo-Responsive Smart Window Derived from Hydrogel. *Joule* **2020**, *4*, 2458–2474. [[CrossRef](#)]
11. Zhang, Y. VO₂(B) conversion to VO₂(A) and VO₂(M) and their oxidation resistance and optical switching properties. *Mater. Sci.* **2016**, *34*, 169–176. [[CrossRef](#)]
12. Cui, Y.; Ke, Y.; Liu, C.; Chen, Z.; Wang, N.; Zhang, L.; Zhou, Y.; Wang, S.; Gao, Y.; Long, Y. Thermochromic VO₂ for Energy-Efficient Smart Windows. *Joule* **2018**, *2*, 1707–1746. [[CrossRef](#)]
13. Liu, C.; Long, Y.; Magdassi, S.; Mandler, D. Ionic strength induced electrodeposition: A universal approach for nanomaterial deposition at selective areas. *Nanoscale* **2016**, *9*, 485–490. [[CrossRef](#)]
14. Vu, T.D.; Liu, S.; Zeng, X.; Li, C.; Long, Y. High-power impulse magnetron sputtering deposition of high crystallinity vanadium dioxide for thermochromic smart windows applications. *Ceram. Int.* **2020**, *46*, 8145–8153. [[CrossRef](#)]
15. Macaluso, R.; Mosca, M.; Costanza, V.; d'Angelo, A.; Lullo, G.; Caruso, F.; Cali, C.; di Franco, F.; Santamaria, M.; di Quarto, F. Resistive switching behaviour in ZnO and VO₂ memristors grown by pulsed laser deposition. *Electron. Lett.* **2014**, *50*, 262–263. [[CrossRef](#)]
16. Liu, C.; Wang, S.; Zhou, Y.; Yang, H.; Lu, Q.; Mandler, D.; Magdassi, S.; Tay, C.Y.; Long, Y. Index-tunable anti-reflection coatings: Maximizing solar modulation ability for vanadium dioxide-based smart thermochromic glazing. *J. Alloys Compd.* **2018**, *731*, 1197–1207. [[CrossRef](#)]
17. Li, M.; Magdassi, S.; Gao, Y.; Long, Y. Hydrothermal Synthesis of VO₂ Polymorphs: Advantages, Challenges and Prospects for the Application of Energy Efficient Smart Windows. *Small* **2017**, *13*, 13–36. [[CrossRef](#)] [[PubMed](#)]
18. Whittaker, L.; Wu, T.-L.; Patridge, C.J.; Sambandamurthy, G.; Banerjee, S. Distinctive finite size effects on the phase diagram and metal–insulator transitions of tungsten-doped vanadium(IV) oxide. *J. Mater. Chem.* **2011**, *21*, 5580–5592. [[CrossRef](#)]

19. Zhou, J.; Xie, M.; Cui, A.; Zhou, B.; Jiang, K.; Shang, L.; Hu, Z.; Chu, J. Manipulating Behaviors from Heavy Tungsten Doping on Interband Electronic Transition and Orbital Structure Variation of Vanadium Dioxide Films. *ACS Appl. Mater. Interfaces* **2018**, *10*, 30548–30557. [[CrossRef](#)]
20. Son, J.-H.; Wei, J.; Cobden, D.; Cao, G.; Xia, Y. Hydrothermal Synthesis of Monoclinic VO₂ Micro- and Nanocrystals in One Step and Their Use in Fabricating Inverse Opals. *Chem. Mater.* **2010**, *22*, 3043–3050. [[CrossRef](#)]
21. Chen, Z.; Gao, Y.; Kang, L.; Cao, C.; Chen, S.; Luo, H. Fine crystalline VO₂ nanoparticles: Synthesis, abnormal phase transition temperatures and excellent optical properties of a derived VO₂ nanocomposite foil. *J. Mater. Chem. A* **2014**, *2*, 2718–2727. [[CrossRef](#)]
22. Alie, D.; Gedvilas, L.; Wang, Z.; Tenent, R.; Engtrakul, C.; Yan, Y.; Shaheen, S.E.; Dillon, A.C.; Ban, C. Direct synthesis of thermochromic VO₂ through hydrothermal reaction. *J. Solid State Chem.* **2014**, *212*, 237–241. [[CrossRef](#)]
23. Li, W.; Ji, S.; Sun, G.; Ma, Y.; Guo, H.; Jin, P. Novel VO₂(M)–ZnO heterostructured dandelions with combined thermochromic and photocatalytic properties for application in smart coatings. *New J. Chem.* **2016**, *40*, 2592–2600. [[CrossRef](#)]
24. Li, D.; Li, M.; Pan, J.; Luo, Y.; Wu, H.; Zhang, Y.; Li, G. Hydrothermal Synthesis of Mo-Doped VO₂/TiO₂ Composite Nanocrystals with Enhanced Thermochromic Performance. *ACS Appl. Mater. Interfaces* **2014**, *6*, 6555–6561. [[CrossRef](#)]
25. Guo, D.; Ling, C.; Wang, C.; Wang, D.; Li, J.; Zhao, Z.; Wang, Z.; Zhao, Y.; Zhang, J.; Jin, H. Hydrothermal One-Step Synthesis of Highly Dispersed M-Phase VO₂ Nanocrystals and Application to Flexible Thermochromic Film. *ACS Appl. Mater. Interfaces* **2018**, *10*, 28627–28634. [[CrossRef](#)] [[PubMed](#)]
26. Malarde, D.; Johnson, I.D.; Godfrey, I.J.; Powell, M.J.; Cibin, G.; Cabrera, R.Q.; Darr, J.A.; Carmalt, C.J.; Sankar, G.; Parkin, I.P.; et al. Direct and continuous hydrothermal flow synthesis of thermochromic phase pure monoclinic VO₂ nanoparticles. *J. Mater. Chem. C* **2018**, *6*, 11731–11739. [[CrossRef](#)]
27. Powell, M.J.; Marchand, P.; Denis, C.J.; Bear, J.C.; Darr, J.A.; Parkin, I.P. Direct and continuous synthesis of VO₂ nanoparticles. *Nanoscale* **2015**, *7*, 18686–18693. [[CrossRef](#)] [[PubMed](#)]
28. Chang, T.; Cao, X.; Long, Y.; Luo, H.; Jin, P. How to properly evaluate and compare the thermochromic performance of VO₂-based smart coatings. *J. Mater. Chem. A* **2019**, *7*, 24164–24172. [[CrossRef](#)]
29. Ke, Y.; Zhang, Q.; Wang, T.; Wang, S.; Li, N.; Lin, G.; Liu, X.; Dai, Z.; Yan, J.; Yin, J.; et al. Cephalopod-inspired versatile design based on plasmonic VO₂ nanoparticle for energy-efficient mechano-thermochromic windows. *Nano Energy* **2020**, *73*, 104785. [[CrossRef](#)]
30. Wang, N.; Duchamp, M.; Xue, C.; Dunin-Borkowski, R.E.; Liu, G.; Long, Y. Single-Crystalline W-Doped VO₂ Nanobeams with Highly Reversible Electrical and Plasmonic Responses Near Room Temperature. *Adv. Mater. Interfaces* **2016**, *3*, 1600164. [[CrossRef](#)]
31. Gui, Z.; Fan, R.; Chen, X.; Wu, Y. A New Metastable Phase of Needle-like Nanocrystalline VO₂·H₂O and Phase Transformation. *J. Solid State Chem.* **2001**, *157*, 250–254. [[CrossRef](#)]
32. Ji, S.; Zhang, F.; Jin, P. Preparation of high performance pure single phase VO₂ nanopowder by hydrothermally reducing the V₂O₅ gel. *Sol. Energy Mater. Sol. Cells* **2011**, *95*, 3520–3526. [[CrossRef](#)]